

ANALYSIS OF 3-D MOSAIC REFLECTIVITY DATA COLLOCATED WITH RESEARCH AIRCRAFT AND SATELLITE DATA: IMPLICATIONS ON IN-FLIGHT ICING

David J. Serke¹, F. McDonough¹ and M. K. Politovich¹
¹National Center for Atmospheric Research, Boulder, Colorado

1. INTRODUCTION

During the winter of 2005, icing research flights were conducted over Ohio and nearby states by NASA Glenn's Twin Otter, the UND Citation and a certification aircraft. Analyses of NSSL's 3-D radar mosaic reflectivity data, co-located in space and time with flight data, suggest that it is possible to provide valuable information about the presence of in-flight icing hazards caused by supercooled liquid droplets with radar reflectivity alone. We theorize that high liquid water contents are often present where small mean particle sizes (either ice or liquid) exist near high reflectivity areas in subfreezing conditions. Detection of these conditions can be accomplished by determining a threshold reflectivity value below which it is likely that mostly smaller particles are present. The dominance of smaller particles is evident in the radar mosaic as reflectivity gaps, depressions and sharp vertical or horizontal gradients in reflectivity. These locations tend to be associated with higher liquid water contents. The use of the reflectivity threshold as well as pattern recognition software could provide upgrades to the FAA's Current Icing

Product (CIP) (Bernstein et al., 2005) which detects in-flight icing hazards. Several examples using combinations of NEXRAD 3D mosaic and research aircraft data will be presented to illustrate the utility of this method.

2. DATA

The 3-D National Radar Mosaic product derived at NSSL applies base reflectivity data from the 130 NEXRAD sites to a 1 x 1 km horizontal and 31 vertical level resolution Cartesian grid (Zhang et al., 2004).

The Twin Otter aircraft had a CSIRO and a Nevzorov liquid water content (LWC) probe along with a FSSP particle probe and a 2D-Grey (2D-G) particle probe mounted under its wings. Descriptions of these probes can be found in McDonough and Bernstein (2004). One-second of CSIRO and Nevzorov LWC sensor values were compared to each other for consistency. If the values were within 0.05 gm^{-3} of one another for 10 consecutive seconds then a ten-second average of all relevant fields was computed. If each ten-second averaged data point was within two minutes

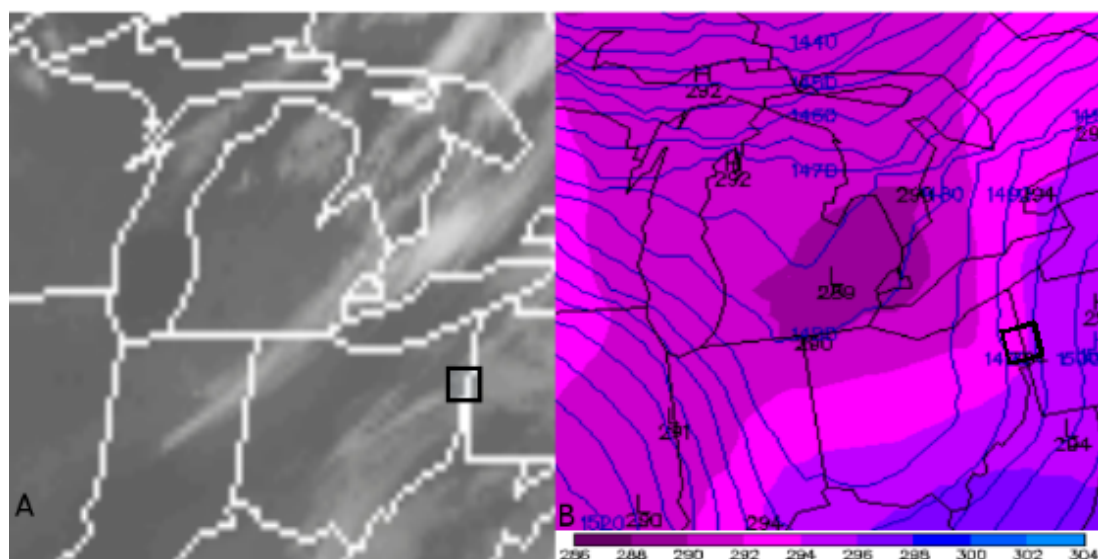


Figure 1: GOES-East visible channel (A) at 1415 UTC and 850 mb analysis (B) of geopotential height (blue contours, [meters]) and equivalent potential temperature (filled colors, [°K]) at 1200 UTC on February 3rd, 2005. The black boxes indicate the case study region.

*Corresponding author address: David J. Serke, National Center for Atmospheric Research, Boulder, CO 80301;
Email: serke@ucar.edu

of the time stamp on a radar mosaic file, the 3-D mosaic was then matched with the aircraft latitude, longitude and altitude (MSL).

The goal of the project forecaster was to direct the aircraft into high LWC areas and to generally avoid environments near high reflectivity regions. Therefore, most flights were into small drop icing cases that occurred nearer the surface. Small -drop dominated clouds are harder to detect at significant range from the radar, and lower altitude flights are more likely to be below a radar's lowest elevation scan angle. The data were analyzed for this research in the context of case studies to best understand the importance of the weather situations and the storm structures.

3. CASE STUDY: FEBRUARY 3rd, 2005

This case study was chosen because it had a constant altitude penetration of a single phase ice crystal cloud with uniformly high reflectivities and low LWC and a second flight leg that traversed a 'reflectivity gap' and then bordered a reflectivity region. The second leg encountered significant LWC

values. A regional overview of the case conditions from Feb 3rd, 2005 is provided within Fig. 1. Part A of the plot is a GOES-East visible image from 14:15 UTC and part B shows geopotential height at 1200 UTC in blue contours with equivalent potential temperature plotted as filled color contours. Together these images depict the passage of a shortwave trough through the midwest with cold advection and some northeast to southwest banded cloud features with the front. The small black box in the visible plot indicates the area where the aircraft was sampling at the time of these images and will be the focus of all successive plots.

The first flight leg was a west-to-east constant altitude penetration at 2.4 km of a nearly uniform region of reflectivities above 10 dBZ (Fig. 2A). The 2D-G probe from 13:53:24 (Fig. 2B, at black 'x') shows long, columnar ice particles mixed with some circular particles roughly 100 μm in diameter. Figure 3 presents the particle size distribution at 13:53:24 which shows the log of particle sizes versus the log of particle concentration with FSSP bins plotted as triangles and 2D-G bins plotted as diamonds. Due to instrument limitations, the sizes between 50 and 100 μm are to be used with caution. A broad maximum

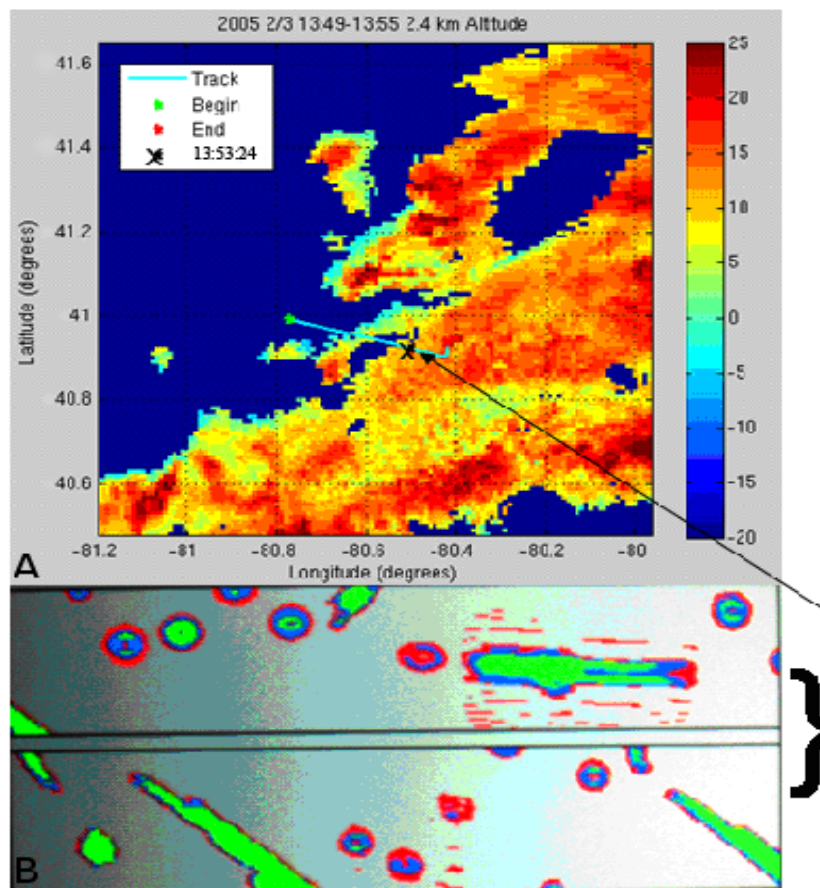


Figure 2: Planview of reflectivity (A, [dBZ]) at 2.4 km altitude from 13:49 to 13:55 GMT on 2/3, 2005 with aircraft track. The 2D-G particle plot at 13:53:24 (B) is shown below the planview.

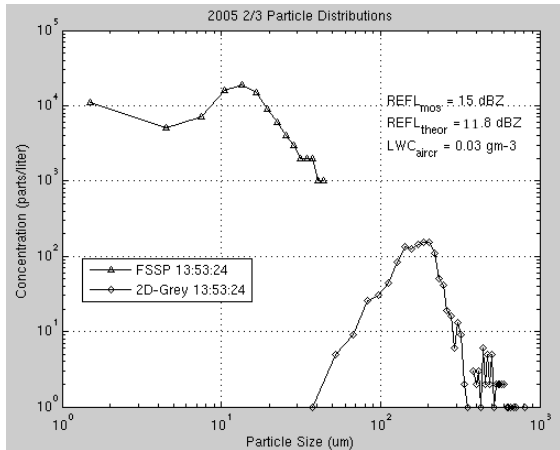


Figure 3: Particle distributions from the FSSP (triangles) and 2D-Grey (diamonds) probes from 13:53:24 (black) correspond to the planview location indicated on figure 2.

near 15 μm represents the cloud-sized particles and a maximum between 150 and 200 microns represents the long columnar ice particles seen in Fig. 2B. The radar equation for liquid targets is

given as:

$$Z = \sum_{i=1}^{FSSP \& 2D-G} D_i^6 * N_i * \Delta D \quad (1)$$

where Z is reflectivity factor, D_i is the diameter of bin i , N_i is the number or particle concentration in bin i and ΔD is the bin width. In an all-ice environment, the returned power is about 7 dB less than if the radar was viewing liquid precipitation (Rinehart, 2004). This calculation yields a reflectivity of 11.8 dBZ, whereas the observed value was 15 dBZ.

The vertical structure, as represented by the closest RUC model (Benjamin, et al., 1998) gridpoint data to the aircraft's location and time, is compared to several reflectivity profiles within the gridbox in Fig. 4. All of the profiles show relatively high reflectivities below and up to the flight level (triangles) with a gradual rate of decrease within the cloud layer. The low LWC values are shown next to the profile times (Fig. 4D) in units of gm^{-3} .

The second flight leg (Fig. 5) was from 14:00 to 14:05 UTC and was just north of the the

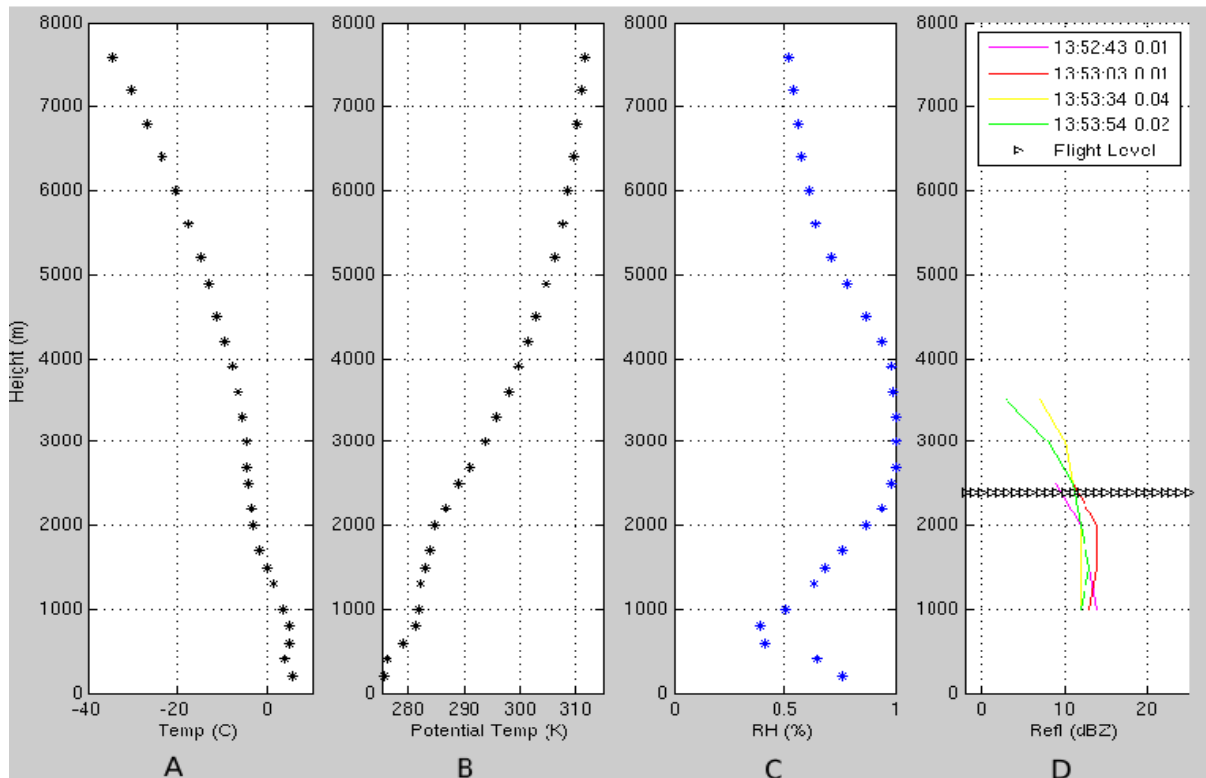


Figure 4. RUC gridpoint temperature (A), derived potential temperature (B), RUC relative humidity (C) mean 3D mosaic reflectivity profiles (D) for times indicated within the RUC gridpoint. The aircraft flight level is indicated with black triangles and the CSIRO LWC (gm^{-3}) is shown next to the profile time.

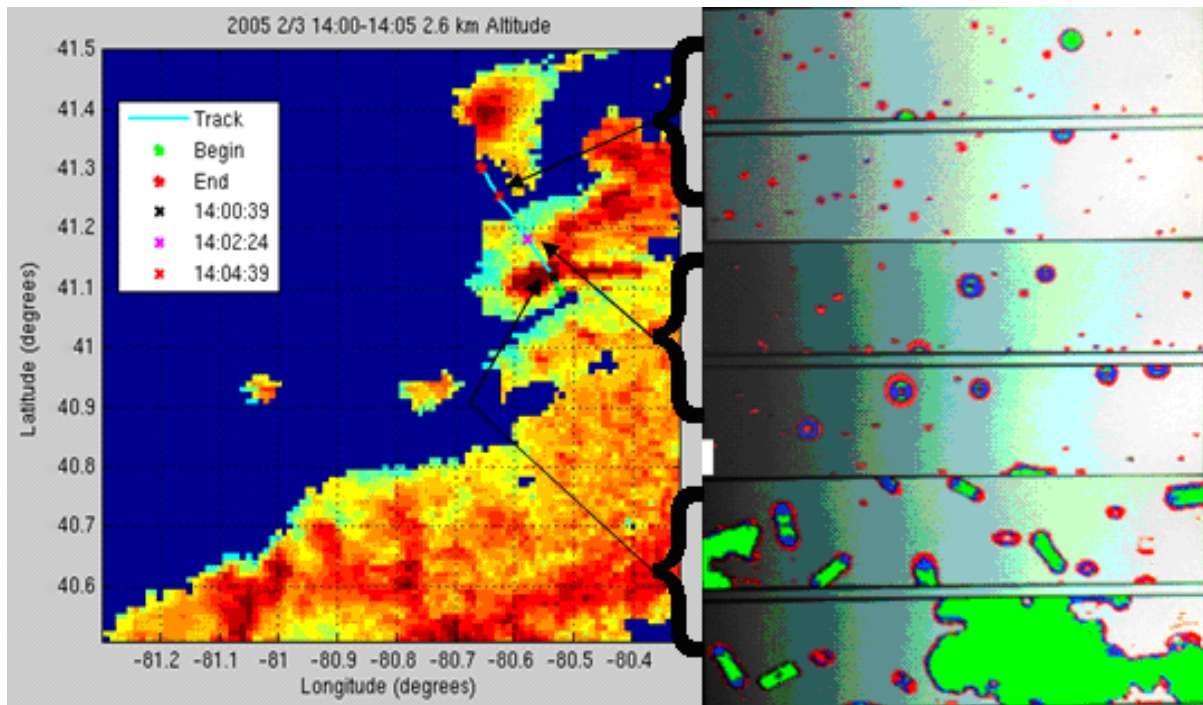


Figure 5. Planview of reflectivity (left, [dBZ]) at 2.6 km altitude from 14:00 to 14:05 GMT on 2/3, 2005 with aircraft track (light blue line from green to red star). The right side of the plot shows 2D-G images each ~0.5 seconds wide and 950 μm high of cloud particles corresponding to the positions and times indicated by the black arrows.

first leg. The cloud microphysics are explored at three times along the leg: high reflectivity (14:04:39, black 'x'), low but detectable reflectivity (14:02:24, magenta 'x') and a location just outside of the minimum detectable reflectivity values, red 'x'. Figure 6 shows the combined FSSP and 2D-G particle size distribution at each time. The black 'x' sample was within a cell of reflectivity greater than 20 dBZ. The 2D-G imagery (Fig. 5B) depicts many crystalline barrel shapes and some larger aggregates. A broad peak depicting cloud drop

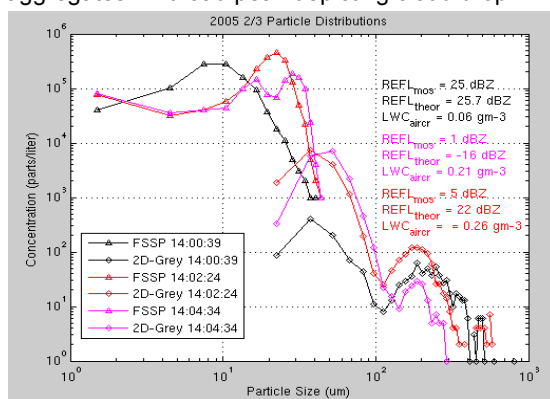


Figure 6: Particle distributions from the FSSP (triangles) and 2D-Grey (diamonds) probes from 13:53:24 (black) correspond to the planview location indicated on Fig 2.

sizes of around 10 μm dominates the concentration at this time.

A small number of large (200-700 μm) aggregates contributed the most to the high reflectivity. The magenta 'x' is in an area of low reflectivity with significant LWC of 0.21 gm^{-3} near a reflectivity gap. The 2D-G imagery shows spherical particles of size 100 μm or less and some smaller cloud-sized particles that are not fully illuminated. The red 'x' is in a reflectivity gap where the reflectivity is below the minimum detectable by the radar but the LWC is 0.26 gm^{-3} . The 2D-G shows mostly small particles with a few spherical particles of less than 100 μm . Both the magenta and red sampling times have maximum concentrations shifted to larger sizes (30 versus 10 μm) than the black sampling time and had elevated concentrations between 15 and 100 μm .

Figure 7 presents a timeseries of 3D mosaic reflectivity (top) and LWC (bottom) along the second flight leg. The relation of reflectivity to LWC is shown for the three sampling times (black, magenta and red). Lower (higher) reflectivities generally had higher (lower) LWC values in this post-cold frontal scenario.

The RUC temperature and humidity fields for the gridbox which includes the second flight leg (Fig. 8) are little changed from the first flight leg. The model is showing a cloud (area of

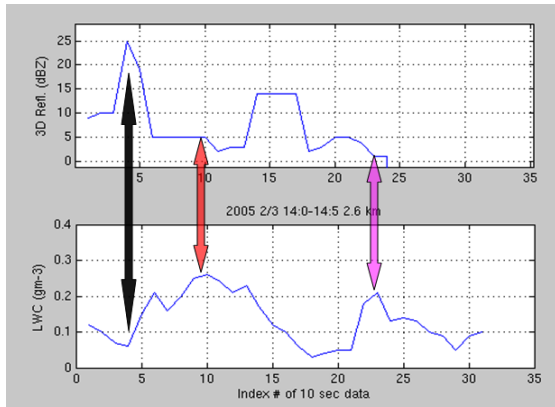


Figure 7: 3D mosaic reflectivity (top, dBZ) and LWC (bottom, gm^{-3}) during the second flight leg. Colored arrows indicate the time of each sample discussed previously.

approximately 100% relative humidities) between 2 and 4 km altitude. Within the RUC gridbox, a wide range of LWCs and reflectivity soundings exist. The far right panel of Fig. 8 shows several reflectivity profiles from the reflectivity gap at the start of the second leg (red), across the high reflectivity cell (green) and then toward the reflectivity gap to the north (black).

4. SUMMARY

Comparison of the NASA Glenn Twin Otter meteorological and microphysical data to NSSL's National 3-D reflectivity mosaic reveals that important information about the threat of in-flight icing can be derived. First, temperatures typically have to be between 0 to -20 degrees Celsius for icing to occur. The above results suggest that reflectivities below 5 dBZ are indicative of higher (greater than $0.2 gm^{-3}$) LWCs in a post-cold frontal cold season scenario. Reflectivities above 10 dBZ tend to be associated with lower LWCs. The existence of supercooled liquid drops is a delicate balance between the production of supercooled water and its depletion via ice crystal scavenging.

Analysis of this case and four other cases during the cold season in the midwest US (not shown) has led to the following observations:

- Regions of uniform reflectivity above 10 dBZ tend to have low LWC.
- Reflectivity 'depressions' (area less than 5 dBZ) within uniformly high reflectivity areas had high LWC values.
- Gaps in reflectivity below the minimum detectable often had high LWC.

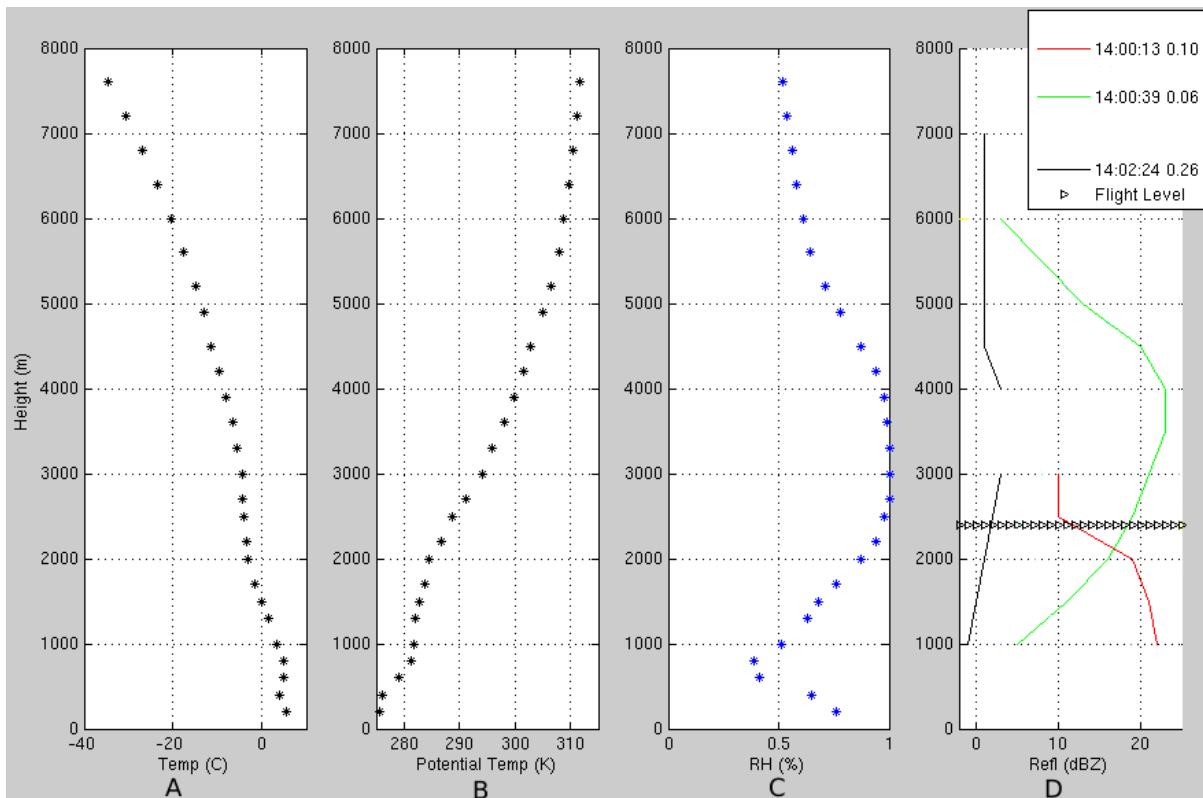


Figure 8. RUC gridpoint temperature (A), derived potential temperature (B), RUC relative humidity (C) and 3D mosaic reflectivity profiles (D) for times indicated within the RUC gridpoint. The aircraft flight level is indicated with black triangles and the Kingprobe LWC (gm^{-3}) is shown next to the profile time.

- Transitions along reflectivity feature edges sometimes exhibited significant LWC.
- Regions with reflectivity greater than 5 dBZ situated above active convection often had high LWC.

These observations led to the following hypotheses/conclusions:

- Regions of uniform reflectivity above 10 dBZ tend to have low LWC because the larger crystals 'scavenge' out much of the available LWC by the Bergeron process.
- Reflectivity gaps and depressions were regions where smaller supercooled droplets dominate and the scavenging process was not active.
- Transitions along reflectivity feature edges sometimes exhibit high LWC, especially in cases when the edge was in the wake of precipitation. This could be due to the immediate post-cold frontal airmass being relatively devoid of ice nuclei. This 'clean' airmass characteristic in association with the shallow convective nature of the post-frontal airmass likely contributed to the enhanced presence of supercooled liquid along these reflectivity edge locations.

The results shown from analyzing these case studies have the potential to improve CIP. A great deal of new information is available to CIP with the vertical dimensionality and increased spatial and temporal resolution of the 3D radar mosaic. Further research into the shapes and lapse rate of the reflectivity profiles may yield information on probable types of precipitation reaching the ground as well as the of in-flight icing conditions.

5. ACKNOWLEDGEMENTS

This research is in response to requirements and funding by the Federal Aviation Administration (FAA). The views expressed are those of the authors and do not necessarily represent the official policy or position of the FAA.

6. REFERENCES

- Benjamin, S.G., J.M. Brown, K.J. Brundage, B.E. Schwartz, T.G. Smirnova, and T.L. Smith, 1998: The operational RUC-2. Preprints, 16th Conference on Weather Analysis and Forecasting, AMS, Phoenix, pp. 249-252.
- Bernstein, B. C., F. McDonough, M. K. Politovich, B. Brown, T. Ratvasky, D. Miller, C. Wolff and G. Cuning, 2005: Current Icing Potential: Algorithm Description and Comparison with Aircraft Observations. *J. of Applied Met.*, **44**, 969-986.
- Bernstein, B.C., F. McDonough, C.A. Wolff, M.K. Politovich, R.M. Rasmussen and S.G. Cober, 2004: Diagnosis of supercooled large drop conditions using cloud water content and drop concentration. Paper 8.6, *11th Conf. on Aviation, Range and Aerospace Meteorology*, Hyannis, 4-8 Oct.
- Harrison, E. F.; Young, D. F.; Minnis, P.; Gibson, G. G.; Cess, R. D.; Ramanathan, V.; Murray, T. D.; and Travers, D. J.: Monthly Regional TOA and Surface Radiation Budget (Subsystem 10.0). "Clouds and the Earth's Radiant Energy System (CERES) Algorithm Theoretical Basis Document, Volume IV: Determination of Surface and Atmosphere Fluxes and Temporally and Spatially Averaged Products (Subsystems 5-12)", *NASA RP 1376 Vol. 4*, edited by CERES Science Team, December, 1995, pp. 139-156.
- McDonough, F. and Bernstein B. C., 2004: A case study of a Great Lakes supercooled large droplet icing cloud. *11th Conf. on Aviation, Range, and Aerospace Meteorology*, Hyannis, MA, Oct 3-8.
- Rinehart, R. E., 2004: Radar for Meteorologists 4th edition. Rinehart Publications, Columbia, MO.
- Zhang, J., K. Howard, and J.J. Gourley, 2004: Constructing Three-Dimensional Multiple-Radar Mosaics: Examples of Convective Storms and Stratiform Rain Echoes. *J. Atmos. Oceanic Technol.*, **22**, 30-42.